

PCCP

Accepted Manuscript



This is an *Accepted Manuscript*, which has been through the Royal Society of Chemistry peer review process and has been accepted for publication.

Accepted Manuscripts are published online shortly after acceptance, before technical editing, formatting and proof reading. Using this free service, authors can make their results available to the community, in citable form, before we publish the edited article. We will replace this *Accepted Manuscript* with the edited and formatted *Advance Article* as soon as it is available.

You can find more information about *Accepted Manuscripts* in the [Information for Authors](#).

Please note that technical editing may introduce minor changes to the text and/or graphics, which may alter content. The journal's standard [Terms & Conditions](#) and the [Ethical guidelines](#) still apply. In no event shall the Royal Society of Chemistry be held responsible for any errors or omissions in this *Accepted Manuscript* or any consequences arising from the use of any information it contains.

Li/Ag ratio dependent structure and upconversion photoluminescence of $\text{Li}_x\text{Ag}_{1-x}\text{Yb}_{0.99}(\text{MoO}_4)_2: 0.01\text{Er}^{3+}$ phosphors

Fangrui Cheng¹, Zhiguo Xia^{1,2*}, Xiping Jing³, Ziyuan Wang¹

¹*School of Materials Sciences and Technology, China University of Geosciences, Beijing 100083, China*

²*School of Materials Sciences and Engineering, University of Science and Technology Beijing, Beijing 100083, China*

³*Beijing National Laboratory for Molecular Sciences, State Key Laboratory of Rare Earth Materials Chemistry and Applications, College of Chemistry and Molecular Engineering, Peking University, Beijing 100871, China*

* **Corresponding author:**

Zhiguo Xia

E-mail: xiazg@ustb.edu.cn

School of Materials Sciences and Engineering, University of Science and Technology Beijing, Beijing 100083, China

Tel. : +86-10-8237-7955;

Fax. : +86-10-8237-7955

†Electronic supplementary information (ESI) available: the crystallographic information file (CIF) of $\text{Li}_{0.5}\text{Ag}_{0.5}\text{Yb}_{0.99}(\text{MoO}_4)_2:0.01\text{Er}^{3+}$ sample was presented.

Abstract: A series of double molybdate scheelite-type phosphors $\text{Li}_x\text{Ag}_{1-x}\text{Yb}_{0.99}(\text{MoO}_4)_2:0.01\text{Er}^{3+}$ ($x = 0, 0.1, 0.3, 0.5, 0.7, 0.9, 1.0$) were synthesized by the solid state reaction method, and their crystal structures and upconversion (UC) luminescence properties were investigated in detail. The phase structure evolution of this series samples was discussed and the selected $\text{Li}_{0.5}\text{Ag}_{0.5}\text{Yb}_{0.99}(\text{MoO}_4)_2:0.01\text{Er}^{3+}$ was analyzed based on the Rietveld refinement. The UC emission properties and the related UC mechanism were also studied. With increasing Li/Ag ratio in this host, the UC emission intensities of $\text{Li}_x\text{Ag}_{1-x}\text{Yb}_{0.99}(\text{MoO}_4)_2:0.01\text{Er}^{3+}$ increased obviously, and the enhancement could be attributed to the coupling effect and the nonradiative transition between two energy levels of $\text{Li}_x\text{Ag}_{1-x}\text{Yb}(\text{MoO}_4)_2$ matrices and the activator Er^{3+} , which have been also analyzed based on the results from the ultraviolet-visible diffuse reflection spectra (UV-vis DRS) and Raman spectra.

1. Introduction

The researches on rare-earth ions doped upconversion (UC) photoluminescence (PL) materials have currently gained much attention due to their potential applications in many advanced technology fields, such as three-dimensional display,¹ optical data storage,² UC lasers,³⁻⁴ temperature sensors,⁵ DNA detection and biological analyses as biolabels,⁶⁻⁸ and so on. In order to fulfill the corresponding demands in such various application fields, many new UC materials and the related phenomena were reported. For example, the fluoride-based UC phosphors have attracted much attention and have been widely studied due to the low phonon energies of the fluoride compounds.⁹⁻¹² However, the applications of the fluoride-based materials are partly restricted by their low chemical durability and thermal stability.¹³ Therefore, novel oxide-based UC phosphors is essential for the practical applications such as optical displays and sensor devices.¹⁴ In this work, the scheelite structure double molybdates $\text{Li}_x\text{Ag}_{1-x}\text{Yb}(\text{MoO}_4)_2$ possess low lattice vibration energy since it is composed of the heavy metal elements, such as Yb and Mo. Thus, nonradiative transition rates between energy levels of rare earth ions would be low. On the other hand, the present $\text{Li}_x\text{Ag}_{1-x}\text{Yb}(\text{MoO}_4)_2$ host has capacity to accommodate higher content of rare earth ions, because the Yb^{3+} ion is not only commonly used as a favorable sensitizer but also can be easily replaced by other trivalent rare-earth ions due to their similar chemical property.¹⁵

Recently, many studies have also shown that the dopant of Li^+ ion in the UC materials can enhance the UC emission intensity.¹⁶ For example, Bai et al.¹⁷⁻¹⁸ and Chen et al.^{13, 19} reported that the formation of Li^+ -based solution by Li^+ codoping could enhance the UC emissions intensities of $\text{Er}^{3+}:\text{Y}_2\text{O}_3$ and ZnO nanocrystals due to the distortion of crystal field symmetry of Er^{3+} . However, so far, the reason why the dopant of Li^+ ion can enhance the intensity of UC materials is still not clear enough.

In this paper, we studied the crystal structure of $\text{Li}_x\text{Ag}_{1-x}\text{Yb}(\text{MoO}_4)_2:\text{Er}^{3+}$ solid solution. It is found that the dopant of Li^+ ion can change the spectral profiles of the ultraviolet-visible diffuse reflection spectra (UV-vis DRS), UC and Raman spectra of the $\text{Li}_x\text{Ag}_{1-x}\text{Yb}(\text{MoO}_4)_2:\text{Er}^{3+}$ phosphors, and the corresponding mechanism on the enhancement of the UC emission was also discussed.

2. Experimental

The compositions of the prepared samples were $\text{Li}_x\text{Ag}_{1-x}\text{Yb}_{0.99}(\text{MoO}_4)_2:0.01\text{Er}^{3+}$ ($x = 0, 0.1, 0.3, 0.5, 0.7, 0.9, 1.0$). Li_2CO_3 (A.R.), AgNO_3 (A.R.), Mo_2O_3 (A.R.), Yb_2O_3 (99.99%), Er_2O_3 (99.99%) were selected as the starting materials. The stoichiometric mixtures were mixed and ground thoroughly, and then calcinated in air at 650-750°C for 12h.²⁰ The phase structures of the as-synthesized materials were determined by X-ray powder diffraction (XRD) (Rigaku D/max-rB X-ray diffractometer (Tokyo, Japan) with a Cu K α (40KV, 100mA) incident source in the 10–70° 2θ range (0.02°, 2θ step size and 1 s per step)). UV-vis DRS were performed on a UV–Vis–NIR spectrophotometer (UV-3600, Shimadzu), and BaSO_4 served as a reference standard. The upconversion emission spectra were recorded by using a FluoroLog-3 spectrophotometer (HORIBA JOBINYVON, France) equipped with an external power-controllable 980 nm semiconductor laser (Beijing Viasho Technology Company, China). The Raman spectra were recorded on a LabRAM ARAMIS micro-Raman spectrometer (HORIBA JOBINYVON, France) with an excitation laser beam at 638 nm. The measurements were taken in backscattering configuration using a microscope with a 50 \times objective and a laser focal spot of $\sim 1\mu\text{m}^2$.

3. Results

3.1. Phase Analysis and Structure

$\text{Li}_{0.5}\text{Ag}_{0.5}\text{Yb}_{0.99}(\text{MoO}_4)_2:0.01\text{Er}^{3+}$ phosphor was firstly chosen as a typical case from a series of solid-solutions $\text{Li}_x\text{Ag}_{1-x}\text{Yb}_{0.99}(\text{MoO}_4)_2:0.01\text{Er}^{3+}$ ($x = 0, 0.1, 0.3, 0.5, 0.7, 0.9, 1.0$) suggesting the detailed characteristics of the crystal structure. Therefore, **Fig. 1 (a)** shows the Rietveld refinement patterns of the $\text{Li}_{0.5}\text{Ag}_{0.5}\text{Yb}_{0.99}(\text{MoO}_4)_2:0.01\text{Er}^{3+}$ sample, and the inset shows the representative crystal structure. Considering the formation of the iso-structural phases, the crystal structure of $\text{LiYb}(\text{MoO}_4)_2$ phase was taken as starting model for Rietveld refinement. The fractional atomic coordinates and isotropic displacement parameters (\AA^2) of $\text{Li}_{0.5}\text{Ag}_{0.5}\text{Yb}_{0.99}(\text{MoO}_4)_2:0.01\text{Er}^{3+}$ obtained from the Rietveld refinement are shown in **Table 1**, and the crystallographic information file (CIF) was presented in electronic supplementary information (ESI). Moreover, the crystallographic data, as well as the data from the two end members of $\text{LiYb}(\text{MoO}_4)_2$ and $\text{AgYb}(\text{MoO}_4)_2$, are also listed in **Table 2** as a comparison.²¹⁻²² Based on the above data, one can see that the structure of $\text{Li}_{0.5}\text{Ag}_{0.5}\text{Yb}_{0.99}(\text{MoO}_4)_2:0.01\text{Er}^{3+}$ was assigned to the crystalline tetragonal system with space group $I-4(82)$. The refinement lattice parameters and residual factors of $\text{Li}_{0.5}\text{Ag}_{0.5}\text{Yb}_{0.99}(\text{MoO}_4)_2:0.01\text{Er}^{3+}$ are listed in Table 2. As for this kind of scheelite-type double molybdate shown in the inset of **Fig.1(a)**, the Er^{3+} and alkali metal Li^+ ions arbitrarily substitute for Yb^{3+} and Ag^+ ions in the host lattice. What's more, in the host of $\text{AgYb}(\text{MoO}_4)_2$, the positions of the Yb^{3+} and Ag^+ ions are randomly distributed. Hence, the four oxygen atoms surrounding the Mo^{6+} ions to

form isolated $[\text{MoO}_4]^{2-}$ tetrahedron, while the cations of Li^+ , Ag^+ , Yb^{3+} , Er^{3+} are arbitrarily distributed among the isolated $[\text{MoO}_4]^{2-}$ tetrahedrons and replace each other.

This series of solid solutions $\text{Li}_x\text{Ag}_{1-x}\text{Yb}_{0.99}(\text{MoO}_4)_2:0.01\text{Er}^{3+}$ ($x = 0, 0.1, 0.3, 0.5, 0.7, 0.9, 1.0$) samples were selected and the XRD patterns were shown in **Fig.1 (b)**. All the diffraction peaks of the seven products can be readily indexed to the pure tetragonal phase of $\text{AgYb}(\text{MoO}_4)_2$ or $\text{LiYb}(\text{MoO}_4)_2$. Since $\text{AgYb}(\text{MoO}_4)_2$ and $\text{LiYb}(\text{MoO}_4)_2$ share the same crystal structure, i.e., tetragonal with the same space group of $I-4$ (No. 82), the solid solution phase of these samples maintained a tetragonal crystal structure. Based on the different Li/Ag ratio in the host, the crystal structure was retained due to the similar characteristics of Ag^+ and Li^+ . It also indicates that Li^+ can be substituted for Ag^+ , forming a full-range continuous solid solution of molybdates. In addition, only the diffraction peaks from scheelite phase can be observed suggesting that Er^{3+} was effectively doped into the host lattice to substitute the Yb^{3+} sites. There are obvious shifts of the diffraction peak (112), (004), (200) depending on the different Li/Ag ration as shown in the inset of **Fig.1(b)**. This is due to the different ionic radius values of Li^+ (0.92) and Ag^+ (1.28) in the eight coordination, also meaning that $\text{Li}_x\text{Ag}_{1-x}\text{Yb}_{0.99}(\text{MoO}_4)$ solid solutions are successfully synthesized and the cell volume can be adjusted. Furthermore, the tetragonality ($c/2a$) of this series of $\text{Li}_x\text{Ag}_{1-x}\text{Yb}_{0.99}(\text{MoO}_4)_2:0.01\text{Er}^{3+}$ samples as a function of x is plotted as shown in **Fig.1 (c)**. As x values vary from 0 to 1.0, the tetragonality $c/2a$ ratio decreases in linear dependence from 1.09954 to 1.08492 and the volume of unit cell

also reduces in linear dependence from 305.85 to 289.80 Å³, which obeys to the Vegard's law. The results are also shown in **Table 3**. These results demonstrate that crystalline structure realizes the continuous variation and remains the same tetragonality though the x values varie from 0 to 1.0. However, due to the different ionic radius values of Li⁺ (0.92) and Ag⁺ (1.28) in the eight coordination, the tetragonality $c/2a$ ratio decreases with the more Li⁺ (x) doped in the Li _{x} Ag_{1- x} Yb_{0.99}(MoO₄)₂:0.01Er³⁺ phosphors, which shows unit cell approaching to the cubic.

3.2. UC Luminescence Properties

Fig. 2(a) shows the typical UC emission spectra of the selected Li _{x} Ag_{1- x} Yb_{0.99}(MoO₄)₂:0.01Er³⁺ sample upon the 980 nm laser excitation with the pump power of 2.5 W/cm². The typical UC spectrum consists of the strong green emission bands at 530/553 nm and the weak red band at 656 nm originating from the intra $4f$ - $4f$ electronic transitions $^2H_{11/2}/^4S_{3/2} \rightarrow ^4I_{15/2}$ and $^4F_{9/2} \rightarrow ^4I_{15/2}$ of the Er³⁺ ions, respectively. The observed UC emission is generated through multiple process including ground-state absorption (GSA), excited-state absorption (ESA), cross relaxation (CR) and energy transfer (ET) when excited with 980 nm semiconductor laser. The possible upconversion luminescence mechanism is shown in **Fig.2 (b)**. An Yb³⁺ ion is excited from ground state ($^2F_{7/2}$) to ($^2F_{5/2}$) through GSA process, by absorbing 980 nm photons and then promotes an Er³⁺ ion from $^4I_{15/2}$ to $^4I_{11/2}$ by transferring the energy to it. Then the excited Er³⁺ ion transits to a higher level at $^4F_{7/2}$ when another Yb³⁺ ion at $^2F_{5/2}$ level continuously transfers the energy to it. And then

the Er^{3+} ion at excited state can also be promoted to the $^4\text{F}_{7/2}$ level by absorbing a 980 nm photon through an ESA process. The populated level $^4\text{F}_{7/2}$ decays non-radiatively to $^2\text{H}_{11/2}$ and $^4\text{S}_{3/2}$, finally produces green emissions at 530 nm and 553 nm with a radiative transition to ground state $^4\text{I}_{15/2}$, respectively. It can be concluded that the occurrence of green upconversion can be attributed to a two-photon process. The red UC emission is originated from the transition of $^4\text{F}_{9/2} \rightarrow ^4\text{I}_{15/2}$ of Er^{3+} , and the population of $\text{Er}^{3+} \ ^4\text{F}_{9/2}$ level in the bulk materials is mainly ascribed to the cross relaxation (CR) and energy transfer process. Similarly, Er^{3+} ions can be pumped to the $^4\text{F}_{7/2}$ level via a two-photon process, accordingly, the CR process occurs between the Er^{3+} ions at level $^4\text{F}_{7/2} + ^4\text{F}_{9/2} \rightarrow ^4\text{I}_{11/2} + ^4\text{F}_{9/2}$. Then the red UC emission can be produced owing to the transition of $^4\text{F}_{9/2} \rightarrow ^4\text{I}_{15/2}$ of Er^{3+} . **Fig.2(c)** shows the UC spectra of this series of $\text{Li}_x\text{Ag}_{1-x}\text{Yb}_{0.99}(\text{MoO}_4)_2:0.01\text{Er}^{3+}$ ($x = 0, 0.1, 0.3, 0.5, 0.7, 0.9, 1.0$) phosphors and similar spectral profiles can be observed except for the variation of the emission intensities. Then, the dependence of UC green emission intensities on the Li^+ doping concentration is given in **Fig.2(d)**. With increasing Li/Ag ratio, the integrated green UC emission intensities for $\text{Li}_x\text{Ag}_{1-x}\text{Yb}_{0.99}(\text{MoO}_4)_2:0.01\text{Er}^{3+}$ phosphors is enhanced, as shown in **Fig.2(d)**, and it tends to be saturated at $x = 0.7$, which demonstrates that the introduction of Li^+ can enhance the UC intensities in the present case, and the possible mechanism will be discussed below.

The dependence of UC intensity for four selected compositions of $\text{Li}_x\text{Ag}_{1-x}\text{Yb}_{0.99}(\text{MoO}_4)_2:0.01\text{Er}^{3+}$ ($x = 0, 0.3, 0.7$ and 1) phosphors upon the excitation power of laser diode is shown in **Fig.3**. As we know, the relationship between the UC

intensity (I_{UC}) and the excitation power (P) can be approximately expressed as the following Eq. (1):

$$I_{uc} \propto P^n \quad (1)$$

where n is the number of infrared photons absorbed for emitting a visible photon. In the double-log coordinate graph shown in **Fig.3**, the slope of $I_{uc} - P^n$ indicates the value of n , which is used for the deduction of the possible upconversion luminescence process. When $x = 0$, the values of n for emissions at 530 nm, 553 nm (green light) and 656 nm (red light) are 1.75 and 1.75, respectively. When x varies from 0 to 1, the values of n for emissions at 530 nm, 553 nm (green light) and 656 nm (red light) are both below than 2. The decrease of n due to the competition between linear decay and UC processes for the depletion of the intermediate excited states has been also reported.²³ The UC luminescence intensity for an n -photon energy transfer process was proportional to the n -th power of the excitation power (P^n) in the limit of the infinitely small UC rates, while the intensity was proportional to the excitation power (P^1) in the limit of infinitely large upconversion rates. Therefore, the intensity of UC luminescence excited by the sequential absorption of n photons has a dependence of P^β on absorbed excitation power P with $1 < \beta < n$,²³ which give rise to the phenomenon that the slope coefficient is less than 2 in **Fig.3**. As a result, it can be concluded that the green and red emission of $\text{Li}_x\text{Ag}_{1-x}\text{Yb}_{0.99}(\text{MoO}_4)_2:0.01\text{Er}^{3+}$ ($x = 0, 0.1, 0.3, 0.5, 0.7, 0.9, 1.0$) phosphors are both originated from a two-photon process, which is the same as the above-mentioned UC mechanism discussed in **Fig.2(b)**.

4. Discussion

Fig.4 shows the UV-vis DRS of $\text{Li}_x\text{Ag}_{1-x}\text{Yb}_{0.99}(\text{MoO}_4)_2:0.01\text{Er}^{3+}$ ($x = 0, 0.1, 0.3, 0.5, 0.7, 0.9, 1.0$) and $\text{Li}_x\text{Ag}_{1-x}\text{Yb}(\text{MoO}_4)_2$ ($x = 0, 0.5, 1.0$), respectively. As can be seen from **Fig.4(b)**, the band gaps of $\text{Li}_x\text{Ag}_{1-x}\text{Yb}(\text{MoO}_4)_2$ ($x = 0, 0.5, 1.0$) are obviously different, which should be due to the different electronegativity values of Li^+ (0.91) and Ag^+ (1.87).²⁴ Therefore, it will lead to the different covalent property of host crystal lattice. On the basis of Pankove's²⁵ and Hao's²⁶ suggestion, the reflection spectrum was expressed as the following Eq. (2),

$$(\alpha h\nu)^2 \propto h\nu \quad (2)$$

where α was the reflection coefficient, h was Planck's constant, and ν was the frequency of light. Therefore, the band gap value (E_g) was taken from the low energy edge (the long wavelength edge) of the absorption band in the reflection spectrum. The E_g values of $\text{Li}_x\text{Ag}_{1-x}\text{Yb}(\text{MoO}_4)_2$ ($x = 0, 0.5, 1.0$) are 3.00 eV, 3.21 eV, 3.42 eV, respectively, which are proportional to the content of Li^+ (x) in the host. And from the **Fig.4 (a)**, the band gap value (E_g) was also increasing with increasing x values. Thus, the increasing E_g values were expected to enhance the UC luminescence due to the decrease of covalent property of host crystal lattice.

We try to explain the UC emission intensity difference in this series of $\text{Li}_x\text{Ag}_{1-x}\text{Yb}(\text{MoO}_4)_2$, so that their relationships among the ionic polarizations, deformations ability of the ions and band gap have been analyzed. Meanwhile, the relationship between band gap and UC luminescence intensity has also been studied, as shown in **Fig.5**. It is accepted that the band gap is associated with the polarization

ability of cation and the deformation ability of ions. On one hand, the polarization ability of cation is considered. The stronger the cationic polarization ability is, the greater the covalent bond connects to the anion, which in turn leads to the narrower band gap. For the sake of having a further understanding of the rising E_g value extension with the increasing x values of the $\text{Li}_x\text{Ag}_{1-x}\text{Yb}_{0.99}(\text{MoO}_4)_2:0.01\text{Er}^{3+}$ ($x = 0, 0.1, 0.3, 0.5, 0.7, 0.9, 1.0$) phosphors, the following model is proposed, as given in Eq. (3)

$$\phi_{eff} = Z_{eff} / r \quad (3)$$

In this model, the effective ionic potential (Φ_{eff}) is introduced to measure the polarization ability of cation. In the definition of the effective ionic potential, where Z_{eff} , it is called the effective cationic nuclear charge, r is cationic radius in the corresponding ligand field.²⁷ By the calculation, the effective cationic nuclear charge results of Ag^+ and Li^+ are $\Phi_{\text{Ag}^+} = 3.63$ and $\Phi_{\text{Li}^+} = 1.41$, which indicate the polarization ability of Ag^+ is stronger than that of Li^+ . As shown in **Fig. 5**, compared to $\text{LiYb}_{0.99}(\text{MoO}_4)_2:0.01\text{Er}^{3+}$ system, oxygen ions have more deformation in the $\text{AgYb}_{0.99}(\text{MoO}_4)_2:0.01\text{Er}^{3+}$ system, which will lead to the enhancement of covalent property of Ag-O bond. Hence, in the $\text{Li}_x\text{Ag}_{1-x}\text{Yb}_{0.99}(\text{MoO}_4)_2:0.01\text{Er}^{3+}$ ($x = 0, 0.1, 0.3, 0.5, 0.7, 0.9, 1.0$) phosphors, when Ag^+ is replaced with Li^+ , the band gaps of the $\text{Li}_x\text{Ag}_{1-x}\text{Yb}(\text{MoO}_4)_2$ host become larger, as shown in the **Fig.4**.

On the other hand, the deformation ability of ions should be also considered. In the present $\text{Li}_x\text{Ag}_{1-x}\text{Yb}_{0.99}(\text{MoO}_4)_2:0.01\text{Er}^{3+}$ ($x = 0, 0.1, 0.3, 0.5, 0.7, 0.9, 1.0$) phosphors, the Mo-O bond is the same, hence, the difference between the deformation

ability of Li^+ and Ag^+ is mainly studied. According to the theory of Lewis hard and soft acids and bases,²⁷ the Li^+ possess the two electron configuration, only 1s orbit has two electrons with small ionic radius and high charge density, which is difficult to deform. Hence, the Li^+ is hard acid. While the Ag^+ is the eighteen electron configuration which the outer shell layer contains $4d^{10}$ orbit with large ionic radius and low charge density, so the Ag^+ is soft acid and it is easy to deform. Thus, as shown in **Fig. 5**, the arrows represent the moving direction of the electron cloud, which is also known as the effects of electron cloud expansion,²⁸ the deformation ability of Ag^+ is stronger than that of Li^+ , which lead to that the Ag^+ feedback electron cloud to the Mo-O bond in the $\text{AgYb}_{0.99}(\text{MoO}_4)_2:0.01\text{Er}^{3+}$ system is more obvious than that of Li^+ in the $\text{LiYb}_{0.99}(\text{MoO}_4)_2:0.01\text{Er}^{3+}$ system. Hence, the covalent property of Mo-O bond in the $\text{AgYb}_{0.99}(\text{MoO}_4)_2:0.01\text{Er}^{3+}$ system is stronger than that of $\text{LiYb}_{0.99}(\text{MoO}_4)_2:0.01\text{Er}^{3+}$ system.

Fig.6 gives the Raman spectra of $\text{AgYb}(\text{MoO}_4)_2$ and $\text{LiYb}(\text{MoO}_4)_2$ host material excited at 638nm, which indicates that the maximum phonon energy of $\text{AgYb}(\text{MoO}_4)_2$ and $\text{LiYb}(\text{MoO}_4)_2$ host material almost have no difference. According to the reported papers²⁹, if the doped concentration of rare earth ions and the maximum phonon energy remain the same, the nonradiative transition probabilities (W_{NR}) of the matrices dominate the factors that influencing rare earth ions doped the upconversion luminous intensity. The expression for the nonradiative rate is given by the following Eq. (4)³⁰

$$W_{NR} = C \left[\frac{1}{\exp\left(\frac{hw_p}{kT} - 1\right)} + 1 \right]^{\frac{\Delta E}{hw_p}} \exp\left(\frac{\Delta E \ln \varepsilon}{hw_p}\right) \quad (4)$$

where ΔE is a measure of the relative offset between these levels; ε accounts for the exact nature of the ion-phonon coupling and is insensitive as $\ln(\varepsilon)$ in the formula; the constant C depends on the phonon density of the matrix. w_p refers to the maximum phonon frequency of the host. The impact of crystal lattice on the UC luminescence mainly depends on phonon. For the purpose of discussing the influence of different lattices on the UC luminous intensity, the **Eq. (4)** is introduced. Therefore, as given in Eq. (4), under the constant temperature (T), three factors (w_p , ε and C) affecting the value of W_{NR} are considered. It is also found from **Fig.6** that the maximum phonon energy of $\text{AgYb}(\text{MoO}_4)_2$ and $\text{LiYb}(\text{MoO}_4)_2$ host have no difference, and then the values of ε and C are only considered. As for the present scheelite molybdate matrix, the intensity of ion-phonon coupling (ε) lies on the influence of Li^+ or Ag^+ on the tetrahedron of $[\text{MoO}_4]^{2-}$. Due to the difference of the deformation ability of ions mentioned above, the polarization ability of O^{2-} in the tetrahedron $[\text{MoO}_4]^{2-}$ to the rare earth Er^{3+} becomes greater and the intensity of ion-phonon coupling (ε) is bigger in the $\text{AgYb}_{0.99}(\text{MoO}_4)_2:0.01\text{Er}^{3+}$ system. Moreover, based on Debye approximation, the following Eq. (5) can be reached,

$$C \propto \rho(w)^{\frac{5}{3}} \quad (5)$$

where $\rho(w)$ is the phonon density of state of the matrix.³¹ Therefore a larger phonon density will result in a larger C , implying a greater W_{NR} and a weaker upconversion

luminescence. As shown in **Fig.6**, the maximum phonon frequency peak (881cm^{-1}) in the $\text{LiYb}(\text{MoO}_4)_2$ host material has a weaker intensity and smaller area than the maximum phonon frequency peak (881cm^{-1}) in the $\text{AgYb}(\text{MoO}_4)_2$ host material. For describing conveniently, the maximum energy phonon density is defined that the integrated intensity of the maximum phonon vibration peak is proportional to the integrated intensity of the host Raman Scattering curve. By calculation, the maximum energy phonon density of $\text{AgYb}(\text{MoO}_4)_2$ and $\text{LiYb}(\text{MoO}_4)_2$ are 0.0829 and 0.0735, respectively. This indicates that the phonon density of the $\text{AgYb}(\text{MoO}_4)_2$ host material is much higher than that of $\text{LiYb}(\text{MoO}_4)_2$ host material. Thus, the values of ε and C in the $\text{AgYb}(\text{MoO}_4)_2$ host are greater than that of $\text{LiYb}(\text{MoO}_4)_2$ host. According to **Eq. (4)**, the nonradiative transition probabilities (W_{NR}) in the $\text{AgYb}(\text{MoO}_4)_2$ are greater than that of $\text{LiYb}(\text{MoO}_4)_2$, which can explain the phenomena that the UC luminous intensity of $\text{AgYb}_{0.99}(\text{MoO}_4)_2:0.01\text{Er}^{3+}$ system is weaker than that of $\text{LiYb}_{0.99}(\text{MoO}_4)_2:0.01\text{Er}^{3+}$ system.

Therefore, the UC luminous intensity of $\text{AgYb}_{0.99}(\text{MoO}_4)_2:0.01\text{Er}^{3+}$ system is weaker than that of $\text{LiYb}_{0.99}(\text{MoO}_4)_2:0.01\text{Er}^{3+}$ system, and the unambiguous interpretation can be reached here. As shown in **Fig.5**, the lower edge of the matrix conduction band is much close to the excitation band energy level of Er^{3+} , hence, there may be some kind of coupling between the matrix conduction band and energy level of Er^{3+} , and this coupling may produce a kind of the way of energy loss, which is also called the nonradiative transition, leading to the UC luminescence intensity diminishing. As mentioned previously, the E_g values of $\text{AgYb}(\text{MoO}_4)_2$ and

$\text{LiYb}(\text{MoO}_4)_2$ are 3.00 eV and 3.42 eV, respectively, therefore, the band gap of the $\text{Li}_x\text{Ag}_{1-x}\text{Yb}_{0.99}(\text{MoO}_4)_2:0.01\text{Er}^{3+}$ will be much closer to the energy level gap 2.14-2.48 eV (500-580 nm) of the activator Er^{3+} with increasing Ag/Li ratio. As a typical case, there may be a part of the coupling (the nonradiative transition) between two energy levels of $\text{AgYb}(\text{MoO}_4)_2$ and the activator Er^{3+} . This phenomenon also exists in the Eu^{3+} doped molybdate and tungstate matrix systems.³²⁻³⁴ That's to say, due to the band gap of Li-based material is wider than Ag-based material, we can only know the excited state of Er^{3+} is much closer to the conduction band of Ag^+ . According to Boltzmann distribution, we can qualitatively know that the excited state electron number of Er^{3+} distributes more to the conduction band of Ag^+ , which will cause some energy lose, leading to the lower UC luminescence intensity. However, we cannot make sure the absolute position of Er^{3+} level in the band gaps for the two different kinds materials, thus, the specific numerical values of energy difference between excited state of Er^{3+} and the conduction band of Ag^+ or Li^+ cannot be made out. Hence, the energy coupling between $\text{AgYb}(\text{MoO}_4)_2$ matrix and Er^{3+} has been weakened when Li^+ was introduced in the $\text{Li}_x\text{Ag}_{1-x}\text{Yb}_{0.99}(\text{MoO}_4)_2:0.01\text{Er}^{3+}$ phosphors, and compared to Ag-based end member, the UC luminescence intensities of $\text{Li}_x\text{Ag}_{1-x}\text{Yb}_{0.99}(\text{MoO}_4)_2:0.01\text{Er}^{3+}$ ($x = 0.1, 0.3, 0.5, 0.7, 0.9, 1.0$) phosphors were enhanced.

5. Conclusions

In conclusion, a series of double molybdate scheelite structure UC luminescence

phosphors $\text{Li}_x\text{Ag}_{1-x}\text{Yb}_{0.99}(\text{MoO}_4)_2:0.01\text{Er}^{3+}$ ($x = 0, 0.1, 0.3, 0.5, 0.7, 0.9, 1.0$) were reported. The crystal structure and phase formation of the $\text{Li}_x\text{Ag}_{1-x}\text{Yb}_{0.99}(\text{MoO}_4)_2:0.01\text{Er}^{3+}$ solid solutions was discussed. With increasing Li/Ag ratio, the nonradiative transition between two energy levels of $\text{Li}_x\text{Ag}_{1-x}\text{Yb}(\text{MoO}_4)_2$ host and the activator Er^{3+} has been weakened since the band gaps of the host were enlarged, and then the UC luminescence intensity were enhanced. A new model on the evaluation of the polarization ability of cation has been built to explore the relationship between the UC luminescence intensity and the host. These results could shed light on the research and understanding of luminescence intensity and efficiency enhancement in rare-earth doped luminescence materials.

Acknowledgements

This present work was supported by the National Natural Science Foundations of China (Grant No. No.51002146, No.51272242), Natural Science Foundations of Beijing (2132050), the Program for New Century Excellent Talents in University of Ministry of Education of China (NCET-12-0950), the Fundamental Research Funds for the Central Universities (2011YYL131), Beijing Nova Program (Z131103000413047) and Beijing Youth Excellent Talent Program (YETP0635) and the Funds of the State Key Laboratory of New Ceramics and Fine Processing, Tsinghua University (KF201306).

References

- [1] E.Dowing, L.Hesselink, J.Ralston, R. Macfarlane, *Science*, 1996, **273**, 1185.
- [2] G.Y. Chen, Y. Liu, Y.G. Zhang, G. Somesfalean, Z.G. Zhang, Q. Sun, F.P. Wang, *Appl. Phys. Lett.*, 2007, **91**, 133103.
- [3] F. Liu, E. Ma, D.Q. Chen, Y.L. Yu, Y.S. Wang, *J. Phys. Chem. B.*, 2006, **110**, 20843.
- [4] S. Sivakumar, Van Veggel, C.J.M. Fank, M.Raudsepp, *J. Am. Chem. Soc.*, 2005, **127**, 12464.
- [5] X. Wang, X.G. Kong, Y. Yu, Y.J. Sun, H. Zhang, *J. Phys. Chem. C.*, 2007, **111**, 15119.
- [6] L.Y. Wang, Y.D. Li, *Chem. Commun.*, 2006, 2557.
- [7] F. Vetrone, J.C. Boyer, J.A. Capobianco, A. Speghini, M. Bettinelli, *J. Phys. Chem. B*, 2002, **106**, 5622.
- [8] E. De la Rosa, L.A. Diaz, R.A. Rodriguez, M.A. Meneses, O. Barbosa, P. Salas, *Appl. Phys. Lett.*, 2003, **83**, 4903.
- [9] Y. Wang, W.P. Qin, J. S. Zhang, C.Y. Cao, J.S. Zhang, Y. Jin, *J. Rare Earth*, 2008, **26**, 40.
- [10] W. Lozano B., Cid B. de Araújo, L.H. Acioli, *J. Appl. Phys.*, 1998, **84**, 2263.
- [11] J.Y. Sun, Y. J. Lan, Z.G. Xia, H.Y. Dua, *Opt. Mater.*, 2011, **33**,576.
- [12] P. Du, Z.G. Xia, L.B. Liao, *Mater. Res. Bull.*, 2011, **46**, 543.
- [13] R. Balda, A. Oleaga, J. Fernández, J.M. Fdez-Navarro, *Opt. Mater.*, 2003, **24**, 83.
- [14] S.K. Singh, K. Kumar, S.B. Rai, *Sensors Actuators A-Phys.*, 2009, 14916.

- [15] G.Y. Chen, H.C. Liu, H.J. Liang, G. Somesfalean, Z.G. Zhang. *Solid State Commun.*, 2008, **148**, 96.
- [16] B.S. Cao, Z.Q. Feng, B. Dong, J. Z. Zheng. *Mater. Rev.*, 2009, **23**, 104.
- [17] Y. Bai, K. Yang, Y. Wang, Z. Zhang, Y. Song. *Opt. Commun.*, 2008, **281**, 2930.
- [18] Y.F. Bai, Y.X. Wang, K. Yang, X.R. Zhang, Y.L. Song, Z.Y. Pan, C.H. Wang. *J. Phys. Chem.C*, 2008, **112**, 12259.
- [19] G.Y. Chen, H.C. Liu, G. Somesfalean, Y.Q. Sheng, H.J. Liang, Z.G. Zhang, Q. Sun, F.P. Wang. *Appl. Phys. Lett.*, 2008, **92**, 113.
- [20] V. Volkov, C. Cascales, A. Kling, C. Zaldo. *Chem. Mater.*, 2005, **17**, 291.
- [21] Volkov, V., Cascales, C., Kling, A.; Zaldo, C. *Chem. Mater.*, 2005, **17**, 291.
- [22] M. Rath, Müeller Buschbaum, H. J. *Alloys Compd.*, 1993, **198**, 193.
- [23] M. Pollnau, D.R.Gamelin, S.R.Lüthi, H.U.Güdel, *Phys. Rev. B*, 2000, **61**, 3337.
- [24] Gary L.Miessler, Donald A. Tarr. *I. C.*, Inter. Fourth Edition, Pearson Press, US, 2011,718.
- [25] J. Pankove, *Opt. Processes in Semiconductors*, p. **34**, Prentice-Hall, Inc., Upper Saddle River, NJ, 1971.
- [26] J. Hao, M. Cocivera, *J. Phys. D*, 2002, **35**, 433.
- [27] P. W. Atkins, T.L. Overton, J.P. Rourke, M.T. Weller, F.A. Armstrong. *I. C.*, Fifth Edition.Oxford University Press, New York, 2010, 16.
- [28] S. Shionoya, W.M. Yen, *Phosphor Handbook*, CRC Press, New York, 1998,163.
- [29] Z.M. Yang, Q.Y. Zhang, Y.H. Liu, Z.H. Jiang. *Acta. Phys. Sinica.*, 2005, **5**, 2013.
- [30] D.C. Yeh, W.A. Sibley, M. Suscavage, M.G. Drexhage. *J. Appl. Phys.*, 1987, **62**,

266.

[31] R.C. Powell, *Phys. Solid-State Laser Mater.*, Springer Press, NewYork, 1998,

Chap. 4.

[32] S. Ye, C.H. Wang, X.P. Jing. *J. Electrochem.Soc.*, 2008, **155**, 148.

[33] S. Ye, C.H. Wang, Z.S. Liu, J. Lu, X.P. Jing. *Appl. Phys. B*, 2008, **91**, 551.

[34] S. Ye, C.H. Wang, X.P. Jing. *J. Electrochem.Soc.*, 2009, **156**, 121.

Table captions,

Table 1. Main crystallographic parameters for $\text{Li}_{0.5}\text{Ag}_{0.5}\text{Yb}_{0.99}(\text{MoO}_4)_2:0.01\text{Er}^{3+}$ from the GSAS Rietveld Refinement.

Table 2. Structural parameters for $\text{Li}_{0.5}\text{Ag}_{0.5}\text{Yb}_{0.99}(\text{MoO}_4)_2:0.01\text{Er}^{3+}$ obtained from the GSAS Rietveld Refinement using X-ray powder diffraction data at room temperature.

Table 3. The unit cell parameters of $\text{Li}_x\text{Ag}_{1-x}\text{Yb}_{0.99}(\text{MoO}_4)_2:0.01\text{Er}^{3+}$ ($x = 0, 0.1, 0.3, 0.5, 0.7, 0.9, 1.0$).

Table 1. Fractional atomic coordinates and isotropic displacement parameters (\AA^2) of $\text{Li}_{0.5}\text{Ag}_{0.5}\text{Yb}_{0.99}(\text{MoO}_4)_2:0.01\text{Er}^{3+}$ obtained from the GSAS Rietveld Refinement.

	<i>x</i>	<i>y</i>	<i>z</i>	<i>B</i> _{iso}	Occ.
Li1	1/2	0	1/4	0.30 (19)	0.25
Ag1	1/2	0	1/4	0.30 (19)	0.25
Yb1	1/2	0	1/4	0.30 (19)	0.495
Er1	1/2	0	1/4	0.30 (19)	0.005
Li2	1/2	1/2	0	0.3 (2)	0.25
Ag2	1/2	1/2	0	0.3 (2)	0.25
Yb2	1/2	1/2	0	0.3 (2)	0.495
Er2	1/2	1/2	0	0.3 (2)	0.005
Mo1	0	0	0	0.7 (3)	1
Mo2	0	1/2	1/4	0.7 (2)	1
O1	0.264 (2)	0.857 (3)	0.0802 (11)	0.5 (4)	1
O2	0.224 (3)	0.327 (4)	0.1607 (11)	1.0 (5)	1

Table 2. Main crystallographic parameters for $\text{Li}_{0.5}\text{Ag}_{0.5}\text{Yb}_{0.99}(\text{MoO}_4)_2 \cdot 0.01\text{Er}^{3+}$ from the GSAS Rietveld Refinement and the data from $\text{LiYb}(\text{MoO}_4)_2$ and $\text{AgYb}(\text{MoO}_4)_2$ as comparisons.

Formula	$\text{LiYb}(\text{MoO}_4)_2$ ¹⁹ (ICSD-15228)	$\text{Li}_{0.5}\text{Ag}_{0.5}\text{Yb}_{0.99}(\text{MoO}_4)_2$:0.01Er ³⁺	$\text{AgYb}(\text{MoO}_4)_2$ ²⁰ (ICSD-73062)
Crystal system		tetragonal	
space group		<i>I</i> -4 (82)	
$\alpha=\beta=\gamma,^\circ$		90.0000	
2θ -interval, $^\circ$		5-120	
<i>a</i> (Å)	5.119(1)	5.143(7)	5.180(5)
<i>b</i> (Å)	5.119(1)	5.143(7)	5.180(5)
<i>c</i> (Å)	11.109(3)	11.246(5)	11.366(3)
<i>V</i> (Å ³)	291.11(2)	295.56(8)	305.04(4)
<i>Z</i>		1	
$R_{wp}(\%)$	-	5.57	-
$R_p(\%)$	-	3.75	-
χ^2	-	1.82	-

Table 3. The unit cell parameters of $\text{Li}_x\text{Ag}_{1-x}\text{Yb}_{0.99}(\text{MoO}_4)_2:0.01\text{Er}^{3+}$ ($x = 0, 0.1, 0.3, 0.5, 0.7, 0.9, 1.0$)

x	a	c	$V/\text{\AA}^3$
0	5.181(1)	11.393(6)	305.85(4)
0.1	5.175(1)	11.364(8)	304.38(3)
0.3	5.163(6)	11.314(1)	301.68(2)
0.5	5.143(7)	11.246(5)	295.56(8)
0.7	5.136(1)	11.199(5)	295.44(6)
0.9	5.121(3)	11.132(4)	291.99(7)
1.0	5.111(6)	11.091(4)	289.80(7)

Figure captions

Fig. 1. (a) Powder XRD patterns for Rietveld structure analysis of the selected $\text{Li}_{0.5}\text{Ag}_{0.5}\text{Yb}_{0.99}(\text{MoO}_4)_2:0.01\text{Er}^{3+}$. The solid red lines are calculated intensities, and the crosses are the observed intensities. The short vertical lines show the position of Bragg reflections of the calculated pattern. The blue solid lines below the profiles stand for the difference between the observed and calculated intensities. The inset shows the structure of $\text{Li}_{0.5}\text{Ag}_{0.5}\text{Yb}_{0.99}(\text{MoO}_4)_2:0.01\text{Er}^{3+}$. (b) XRD patterns of as-prepared $\text{Li}_x\text{Ag}_{1-x}\text{Yb}_{0.99}(\text{MoO}_4)_2:0.01\text{Er}^{3+}$ ($x = 0, 0.1, 0.3, 0.5, 0.7, 0.9, 1.0$) phosphors. The standard data for $\text{AgYb}(\text{MoO}_4)_2$ (JCPDS 81-1656) and $\text{LiYb}(\text{MoO}_4)_2$ (ICSD #152282) are also presented in the figure for comparison. The inset shows the variation of diffraction peak of $\text{Li}_x\text{Ag}_{1-x}\text{Yb}_{0.99}(\text{MoO}_4)_2:0.01\text{Er}^{3+}$ ($x = 0, 0.1, 0.3, 0.5, 0.7, 0.9, 1.0$) powders from 28° - 37° . (c) Linear dependence of $c/2a$ ratio and unit cell volume (V) as function of x values in $\text{Li}_x\text{Ag}_{1-x}\text{Yb}_{0.99}(\text{MoO}_4)_2:0.01\text{Er}^{3+}$ ($x = 0, 0.1, 0.3, 0.5, 0.7, 0.9, 1.0$).

Fig. 2. (a) PL spectra of $\text{Li}_{0.5}\text{Ag}_{0.5}\text{Yb}_{0.99}(\text{MoO}_4)_2:0.01\text{Er}^{3+}$ phosphor; (b) Energy level diagram of Er^{3+} - Yb^{3+} ; (c) PL spectra of $\text{Li}_x\text{Ag}_{1-x}\text{Yb}_{0.99}(\text{MoO}_4)_2:0.01\text{Er}^{3+}$ ($x = 0, 0.1, 0.3, 0.5, 0.7, 0.9, 1.0$) phosphors; (d) The dependence of PL intensity on the Li^+ doping concentration.

Fig. 3. Pump power dependence of green upconverted emissions in $\text{Li}_x\text{Ag}_{1-x}\text{Yb}_{0.99}(\text{MoO}_4)_2:0.01\text{Er}^{3+}$: (a) $x = 0$, (b) $x = 0.3$, (c) $x = 0.7$, (d) $x = 1.0$.

Fig. 4. (a) The ultraviolet diffuse reflection spectrum of $\text{Li}_x\text{Ag}_{1-x}\text{Yb}_{0.99}(\text{MoO}_4)_2:0.01\text{Er}^{3+}$ ($x = 0, 0.1, 0.3, 0.5, 0.7, 0.9, 1.0$); (b) the ultraviolet diffuse reflection spectrum of $\text{Li}_x\text{Ag}_{1-x}\text{Yb}(\text{MoO}_4)_2$ ($x = 0, 0.5, 1.0$).

Fig. 5. Electron cloud polarizations and ionic deformations of $\text{AgYb}_{0.99}(\text{MoO}_4)_2$:

0.01Er³⁺ and LiYb_{0.99}(MoO₄)₂:0.01Er³⁺; energy level diagrams of AYb_{0.99}(MoO₄)₂:

0.01Er³⁺ (A = Li or Ag).

Fig. 6. Raman spectra of undoped AgYb(MoO₄)₂ and LiYb(MoO₄)₂ host material excited at 638nm.

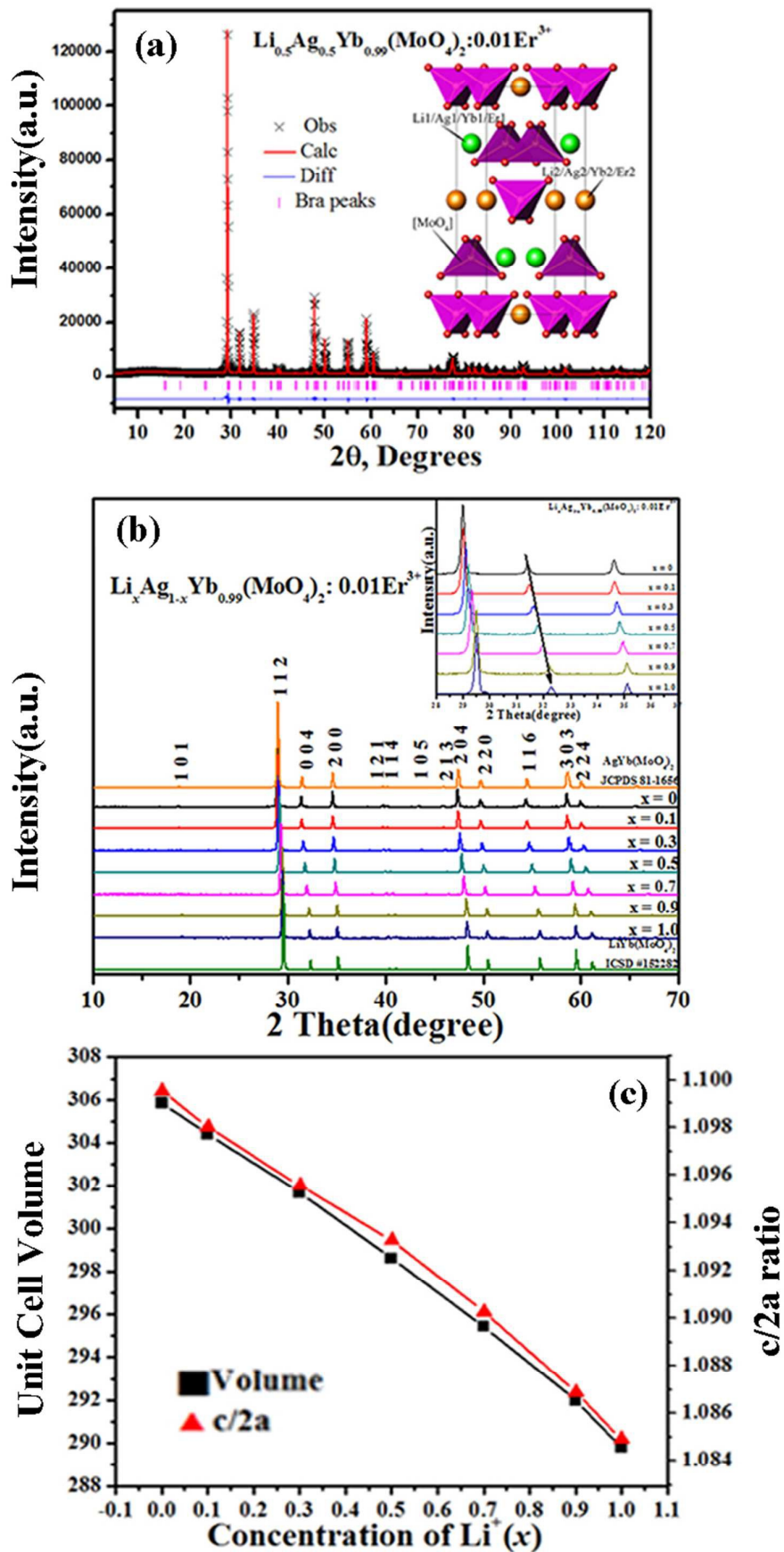


Fig. 1. (a) Powder XRD patterns for Rietveld structure analysis of the selected $\text{Li}_{0.5}\text{Ag}_{0.5}\text{Yb}_{0.99}(\text{MoO}_4)_2:0.01\text{Er}^{3+}$. The solid red lines are calculated intensities, and the crosses are the observed intensities. The short vertical lines show the position of Bragg reflections of the calculated pattern. The blue solid lines below the profiles stand for the difference between the observed and calculated intensities. The inset shows the structure of $\text{Li}_{0.5}\text{Ag}_{0.5}\text{Yb}_{0.99}(\text{MoO}_4)_2:0.01\text{Er}^{3+}$. (b) XRD patterns of as-prepared $\text{Li}_x\text{Ag}_{1-x}\text{Yb}_{0.99}(\text{MoO}_4)_2:0.01\text{Er}^{3+}$ ($x = 0, 0.1, 0.3, 0.5, 0.7, 0.9, 1.0$) phosphors. The standard data for $\text{AgYb}(\text{MoO}_4)_2$ (JCPDS 81-1656) and $\text{LiYb}(\text{MoO}_4)_2$ (ICSD #152282) are also presented in the figure for comparison. The inset shows the variation of diffraction peak of $\text{Li}_x\text{Ag}_{1-x}\text{Yb}_{0.99}(\text{MoO}_4)_2:0.01\text{Er}^{3+}$ ($x = 0, 0.1, 0.3, 0.5, 0.7, 0.9, 1.0$) powders from 28° - 37° . (c) Linear dependence of $c/2a$ ratio and unit cell volume (V) as function of x values in $\text{Li}_x\text{Ag}_{1-x}\text{Yb}_{0.99}(\text{MoO}_4)_2:0.01\text{Er}^{3+}$ ($x = 0, 0.1, 0.3, 0.5, 0.7, 0.9, 1.0$).

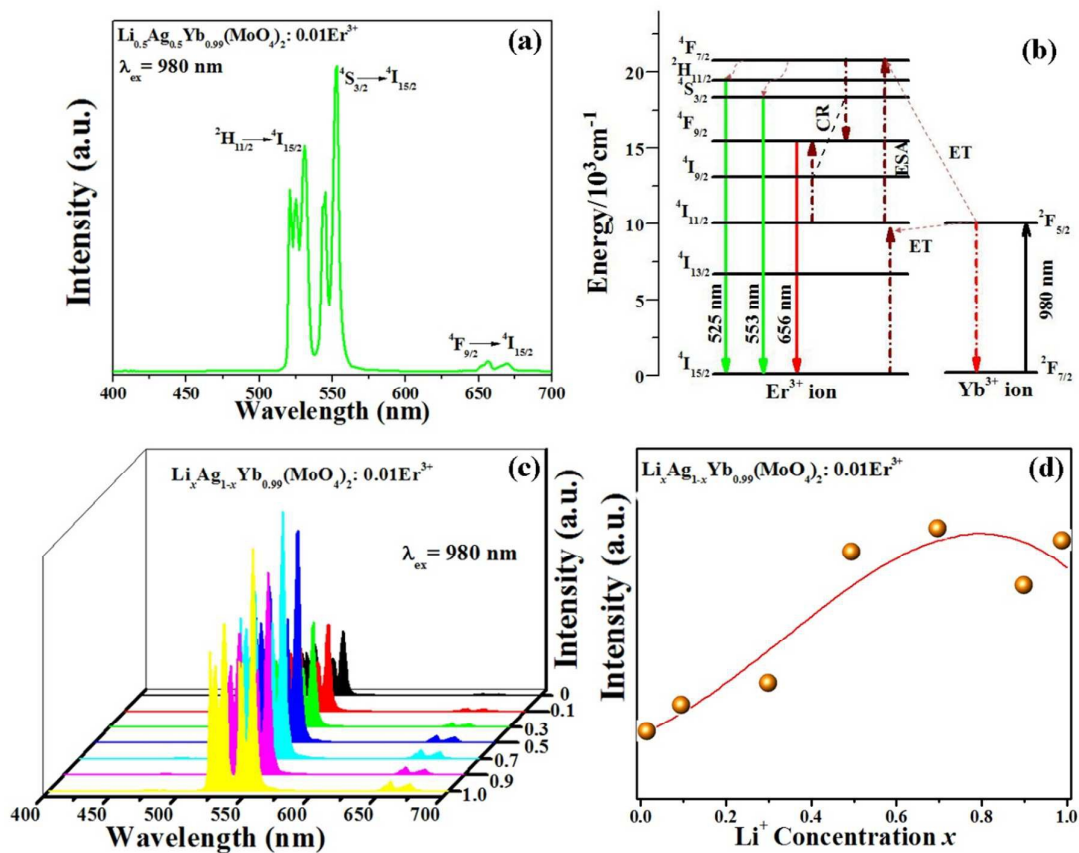


Fig. 2. (a) PL spectra of $\text{Li}_{0.5}\text{Ag}_{0.5}\text{Yb}_{0.99}(\text{MoO}_4)_2:0.01\text{Er}^{3+}$ phosphor; (b) Energy level diagram of $\text{Er}^{3+}-\text{Yb}^{3+}$; (c) PL spectra of $\text{Li}_x\text{Ag}_{1-x}\text{Yb}_{0.99}(\text{MoO}_4)_2:0.01\text{Er}^{3+}$ ($x = 0, 0.1, 0.3, 0.5, 0.7, 0.9, 1.0$) phosphors; (d) The dependence of PL intensity on the Li^+ doping concentration.

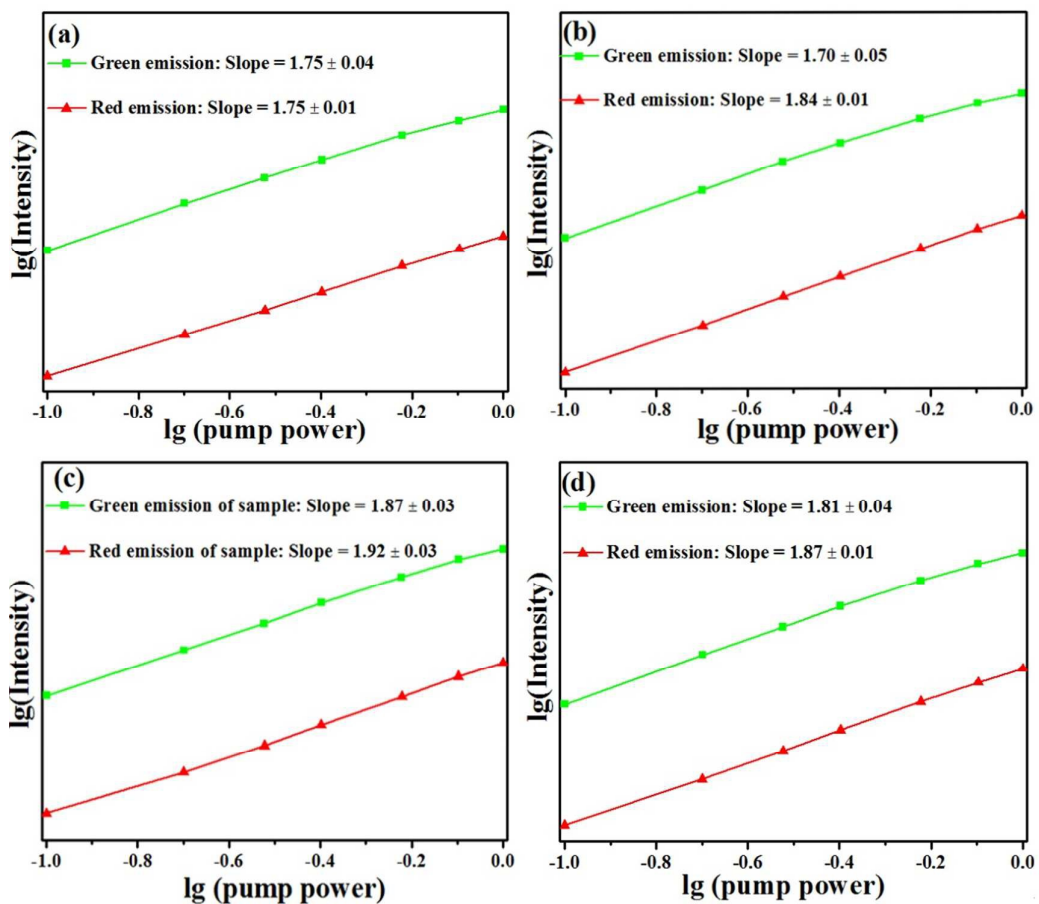


Fig. 3. Pump power dependence of green upconverted emissions in

$\text{Li}_x\text{Ag}_{1-x}\text{Yb}_{0.99}(\text{MoO}_4)_2:0.01\text{Er}^{3+}$: (a) $x = 0$, (b) $x = 0.3$, (c) $x = 0.7$, (d) $x = 1.0$.

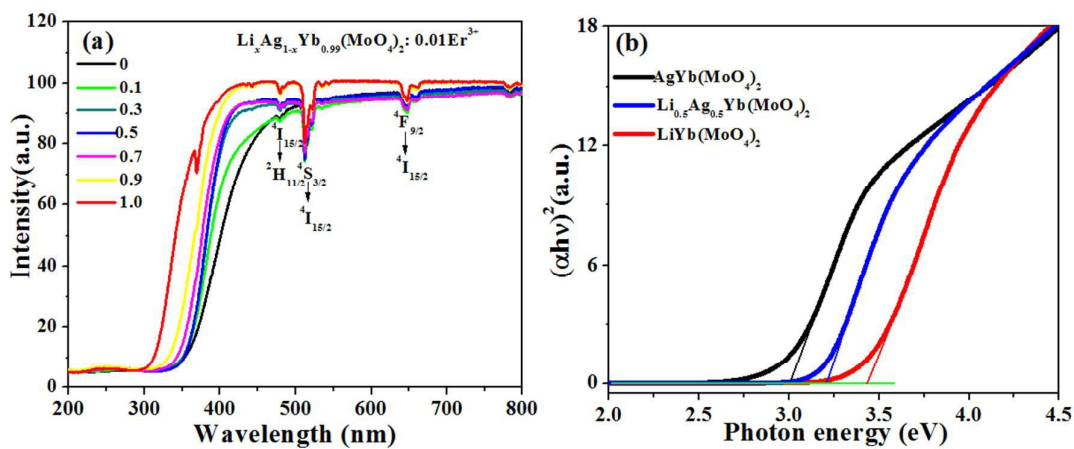


Fig. 4. (a) The ultraviolet diffuse reflection spectrum of $\text{Li}_x\text{Ag}_{1-x}\text{Yb}_{0.99}(\text{MoO}_4)_2:0.01\text{Er}^{3+}$ ($x = 0, 0.1, 0.3, 0.5, 0.7, 0.9, 1.0$); (b) the ultraviolet diffuse reflection spectrum of $\text{Li}_x\text{Ag}_{1-x}\text{Yb}(\text{MoO}_4)_2$ ($x = 0, 0.5, 1.0$).

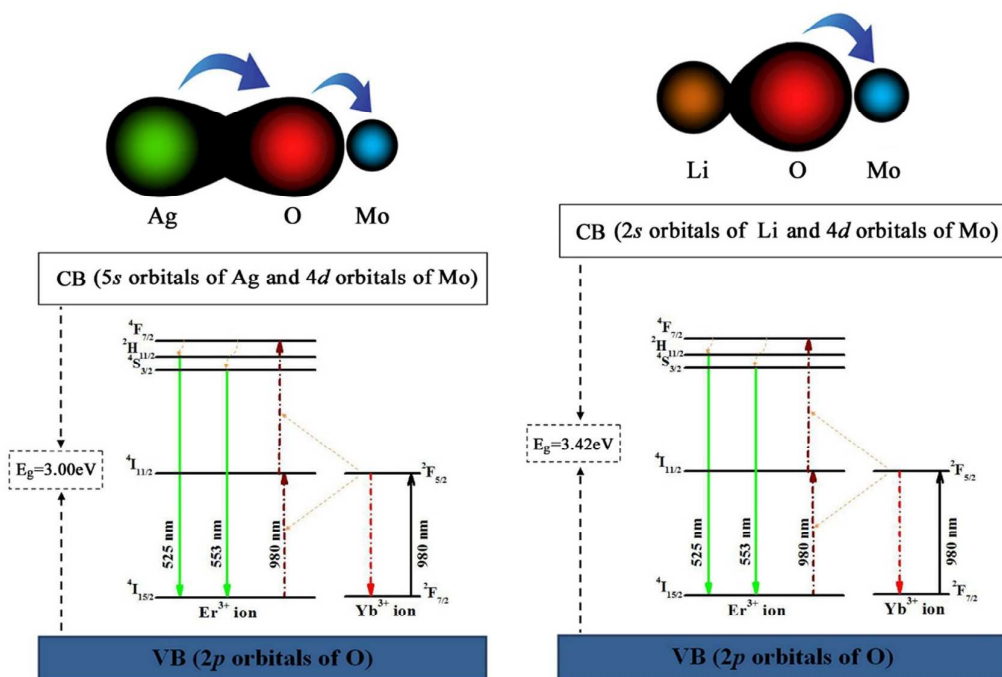


Fig. 5. Electron cloud polarizations and ionic deformations of AgYb_{0.99}(MoO₄)₂:0.01Er³⁺ and LiYb_{0.99}(MoO₄)₂:0.01Er³⁺; energy level diagrams of AYb_{0.99}(MoO₄)₂:0.01Er³⁺ (A = Li or Ag).

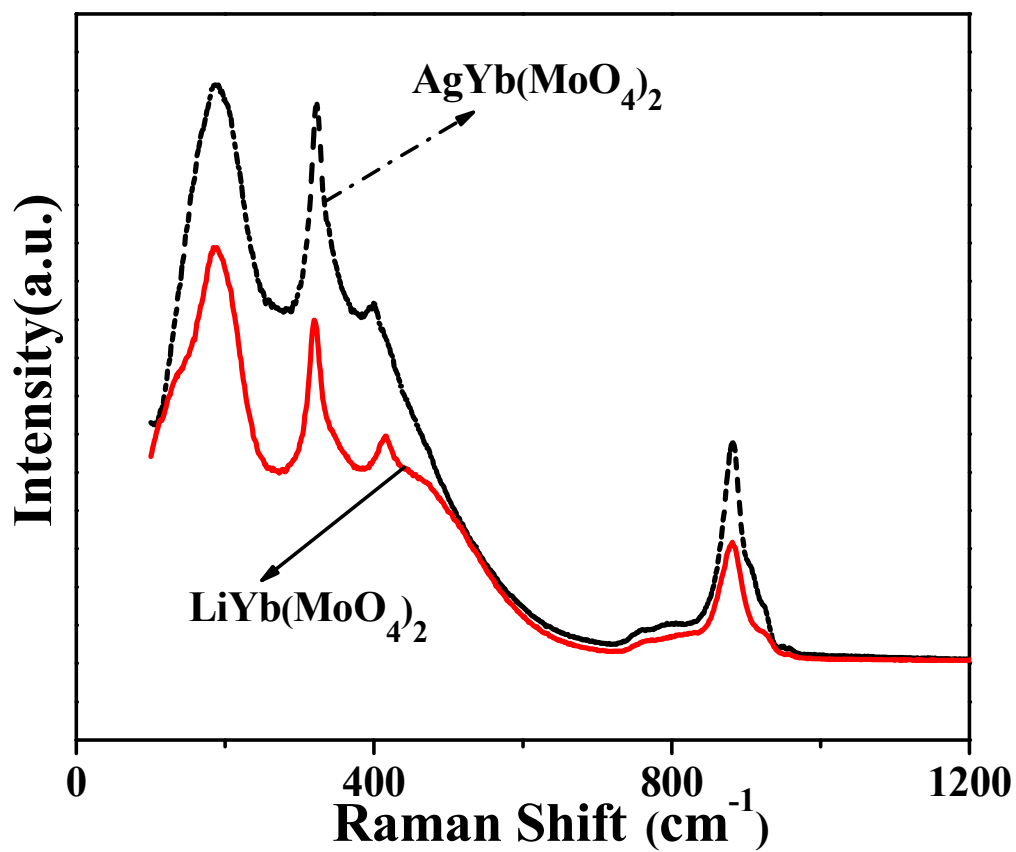


Fig. 6. Raman spectra of undoped $\text{AgYb}(\text{MoO}_4)_2$ and $\text{LiYb}(\text{MoO}_4)_2$ host material excited at 638nm.